Models of Granular Giant Magnetoresistance Multilayer Thin Films

John O. Oti, Stephen E. Russek, Steven C. Sanders and Ralph W. Cross

Abstract—**Phenomenological micromagnetic and large-scale magnetization-dependent models of resistivity that produce giant magnetoresistance in granular multilayer magnetic thin films are described. Included in the models are intralayer and interlayer scattering components formulated explicitly in terms of the microstructural properties and characteristic transport lengths of the medium. The micromagnetic model provides insight into the influence of the magnetization distribution on the giant magnetoresistance response of the medium. The large-scale model which is derived from the micromagnetic model, is useful for obtaining media transport parameters from experimental data. Both models are used to study a set of annealed NiFe/Ag multilayer films.**

I. Introduction

RECENTLY described annealed multilayer (or granular-multilayer) films hold great promise as very sensitive giant magnetoresistance (GMR) materials for read-head designs in ultra-high-density magnetic recording systems [1], [2], [3]. These films are prepared by a method first described by Hylton et al. [1] for a NiFe/Ag system in which a sputtered continuous NiFe/Ag film is subjected to moderate thermal annealing. Due to the immiscibility of the NiFe and Ag phases, Ag penetrates the initially touching NiFe grain boundaries causing the grains to separate from each other. This effect increases with annealing temperature. The grains stack in a columnar structure through the magnetic layers. Magnetization misalignment in the magnetic layers at low fields, which is necessary for GMR, occurs through the relatively weak magnetostatic interactions between the magnetic layers. As a consequence, the saturation field needed to again bring the magnetization of the layers to parallel alignment is much less than those of continuous multilayer films, [4], [5] for which the misalignment mechanism is an antiferromagnetic exchange coupling between the magnetic layers. Slonczewski [6] has shown that magnetostatic interactions in NiFe/Ag systems can lead to complete misalignment of the magnetization of adjacent layers, for intergranular separations of the order of 0.6 to 1 nm. Fig. 1 shows GMR response (relative resistance $\Delta R/R$ versus field) curves of NiFe/Ag granular-multilayer films that we have fabricated, as a function of anneal temperature T. The amplitudes of the $\Delta R/R$ curves first increase with anneal temperature, attaining a maximum at about $T = 340°C$ before decreasing with further increase in temperature (Fig. 1b), and the widths of the $\Delta R/R$ curves increase with temperature. Curves such as the $T = 340°C$ curve of Fig. 1, displaying the largest GMR amplitude of a set of curves obtained for different anneal temperatures, will play important roles in the theory we develop below. These curves will be called *dominant GMR curves*, which are assumed to have almost perfect magnetization misalignment between the layers at zero field.

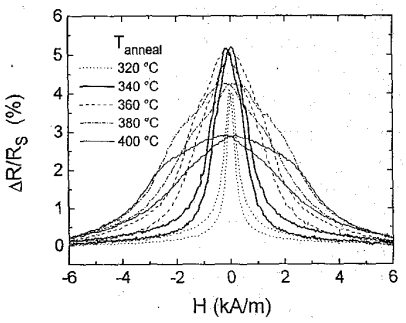

(a)

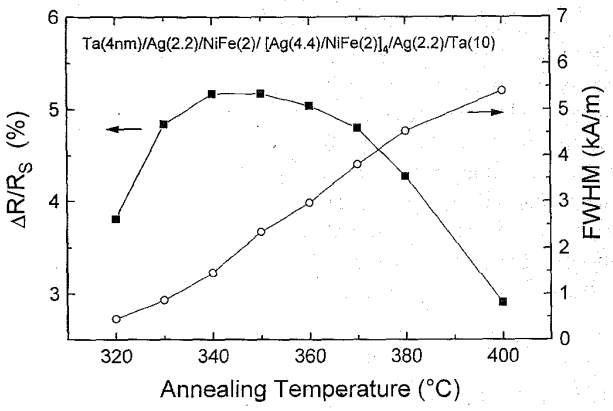

(b)

Fig. 1. (a) GMR response curves of annealed NiFe/Ag multilayers as functions of anneal temperature T; (b) Amplitude and full width at half field maximum (FWHM) of GMR response curves as functions of anneal temperature.

GMR arises from differential spin-dependent scattering

Manuscript received September 30, 1994; revised October 10, 1995.

The authors are with the Electromagnetic Technology Division, National Institute of Standards and Technology, Boulder, Colorado 80303.

Publisher Item Identifier S 0018-9464(96)00875-8.

of conduction electrons as they move through a magnetized material [7]. For GMR to be observed in a multilayer film, the separation between the magnetic layers must be smaller than either the electron mean free path or the electron spin diffusion length depending on the current-flow geometry. Both lengths are temperature dependent. The mean free path measures how far an electron travels in the material without experiencing phonon or impurity scattering which randomizes the electron's momentum, while the electron spin diffusion length measures the distance of travel before an electron's spin is reoriented. Two directions of current flow in the device are usually of interest: The current-in-plane (CIP) direction in which current flows parallel to the film plane, and the current-perpendicular-to-plane (CPP) direction in which current flow is normal to the film plane. The GMR effect is produced by electrons whose spin directions are conserved in making the transition from one magnetic layer to an adjacent layer. Therefore in both CIP and CPP directions, GMR is not observed for interlayer separations greater than the spin diffusion length. Additionally, in the CIP direction, the interlayer separation should remain smaller than the mean free path if GMR is to be observed. For separations larger than the mean free path, the scattering of electrons in the nonmagnetic spacer layers, prevents the electrons from sensing adjacent magnetic layers. The mean free path plays a secondary role in CPP direction, since the current will always pass through the magnetic layers which lie perpendicular to the current path.

Theoretical investigations of GMR can be grouped into two broad categories: The electron transport models and the phenomenological models. Electron transport models use scattering potentials that are obtained from first principles to account for bulk and interface scattering [8]. They are physically realistic but rely on too many parameters that are not always easily ascertained experimentally. In traditional phenomenological models, the modification of the intrinsic resistivity of a multilayer GMR film due to spin-dependent scattering is modeled as being proportional to the cosine of the angle between the magnetization of the magnetic layers [9], [10], [11]. These models correctly predict the nature of the dependence of GMR response on the magnetic state of the medium but do not provide insight into its transport properties. The models we present in this work combine the standard phenomenological approach of modeling resistivity change with an explicit dependence on the microstructural dimensions and characteristic transport lengths of the medium.

The remainder of the article is organized as follows: First a micromagnetic GMR model that takes into account the detailed magnetization state of the medium is described. The micromagnetic model is used to simulate the effects of temperature annealing in NiFe/Ag films. This is followed by the description of a large-scale model derived from the micromagnetic model; the large-scale model is tested using the micromagnetic model. The models are described for the CIP geometry only.

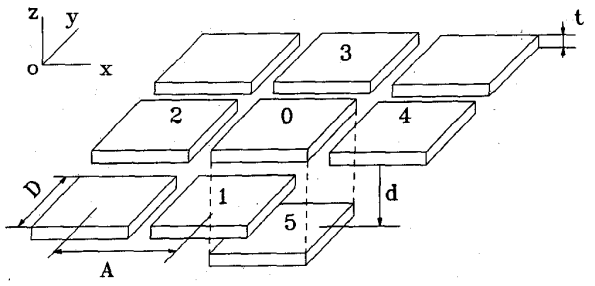

Fig. 2. Schematic of neighboring grains in adjacent layers of a granular multilayer film.

II. Micromagnetic Model

We begin our discussion of the micromagnetic model with Fig. 2, which shows schematically a few neighboring grains of two adjacent magnetic layers of a multilayer film. For ease of discussion, we consider a double-layer film with magnetic layers of equal thicknesses. Generalization to film samples having more than two magnetic layers, and to magnetic layers of unequal thicknesses separated by interlayer separations of different lengths is straightforward. The indicated geometry and associated micromagnetic calculation techniques correspond to those that have been described elsewhere [12]. In the figure, each magnetic grain has a square cross section of length D in the film plane (the x-y plane) and a thickness t in the z direction; A is the distance between the centers of adjacent grains within a magnetic layer and d is the separation between the magnetic layers. A target grain (labeled 0 in Fig. 2) has four nearest neighbors (grains 1–4) within the layer and one nearest neighbor (grain 5) at the corresponding position in the other magnetic layer.

The change in resistivity in an applied field is assumed to have a intralayer component due to electron scattering within a magnetic layer and an interlayer component due to scattering involving two adjacent layers. The interlayer component is proportional to the cosine of the angles between the magnetization of nearest-neighbor grains in adjacent layers. The intralayer component on the other hand is proportional to the cosine of the angles between the magnetization of a grain and its nearest neighbors within a magnetic layer. For simplicity, self-field effects [13] due to current flow in the sample will be neglected in this treatment. The CIP direction will be taken to coincide with the y-axis. The resistivity of the target grain of Fig. 2 for a given magnetization state of the medium is expressed

$$\begin{aligned}\rho &= \rho_s + \delta\rho_r + \delta\rho_l \\ &= \rho_s\{1 + \chi_r\alpha_r[1 - q\hat{\mathbf{m}}_0 \cdot (\hat{\mathbf{m}}_1 + \hat{\mathbf{m}}_2 + \hat{\mathbf{m}}_3 + \hat{\mathbf{m}}_4)] \\ &\quad + \chi_l\alpha_l(1 - \hat{\mathbf{m}}_0 \cdot \hat{\mathbf{m}}_5)\},\end{aligned} \tag{1}$$

where ρ_s is the average resistivity of a grain; $\delta\rho_r$, $\delta\rho_l$ are intralayer and interlayer components of the resistivity change; χ_r, χ_l are intralayer and interlayer material-dependent cofactors; $\alpha_r > 0$, $\alpha_l > 0$ are intralayer and in-

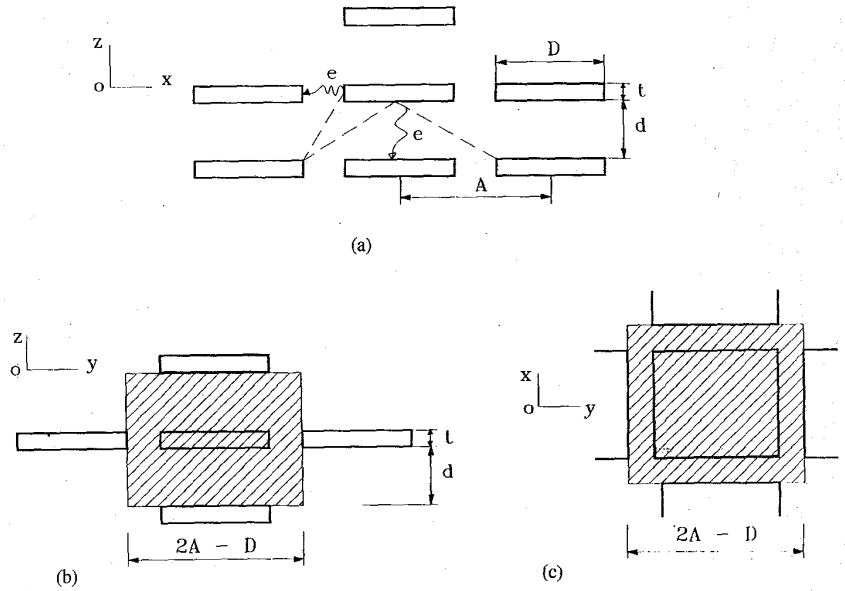

Fig. 3. (a) Cross section of adjacent magnetic layers showing intralayer and interlayer electronic flow (denoted by *e*) among the grains (the rectangles). The dashed lines mark the boundaries of the limiting region inside which an electron originating from the center of the faces is assumed restricted; (b) incidence cross section for intralayer scattering (hatched region); (c) incidence cross section for interlayer scattering (hatched region).

terlayer scattering probability parameters; $\hat{\mathbf{m}}$ is unit magnetization vector; and q is the reciprocal of the number of nearest neighbors of the target grain within a magnetic layer. For double-layer films simulated in this article, $q = 1/4$ and (1) holds. For films having more than two magnetic layers, the expression for the resistivity of a grain in an internal magnetic layer (not shown in Fig. 2), contains the additional term $\rho_s \chi_I \alpha_I (1 - \hat{\mathbf{m}}_0 \cdot \hat{\mathbf{m}}_6)$, to account for an additional neighbor with magnetization $\hat{\mathbf{m}}_6$ in an adjacent magnetic layer. The parameters χ_r, χ_I depend on the intrinsic properties of the medium while α_r, α_I depend on the geometrical properties of its microstructure. As can easily be deduced from (1), $\delta\rho_r$ and $\delta\rho_I$ vanish at saturation when the medium is in a uniformly magnetized state whereupon ρ attains a minimum value ρ_s. The resistivity of a grain attains a maximum of $\rho_s + 2\rho_s\chi_r\alpha_r + 2\rho_x\chi_I\alpha_I$ if its magnetization is directed antiparallel to those of its nearest neighbors. The resistance of each grain can be found from its resistivity by use of the formula (resistivity $\times$ length)/area, which yields ρ/t in the CIP direction.

We shall now derive expressions for the scattering parameters α_r and α_I. These expressions will explicitly contain the microstructural and transport properties of the medium. The forms these dependencies take are arrived at by means of a heuristic treatment of electron transport in the medium. All references to an electron in the discussion are in the statistical sense.

Electronic flow within a magnetic layer and between layers are shown schematically in Fig. 3(a). It is assumed that the most significant scattering events are those occurring between the surfaces of nearest neighbors. As pointed out above, the degree to which an electron originating from a face is scattered between grains is determined by either the mean free path or the electron spin diffusion length. Call such a limiting characteristic length λ; then, to a first approximation the probability of an electron originating from one magnetic site and undergoing spin-dependent scattering at another magnetic site a distance w away can be considered proportional to $\exp(-w/\lambda)$. The probabilities of intralayer and interlayer scattering then are dependent respectively on $\exp(-g/\lambda)$ and $\exp(-d/\lambda)$, where $g = A - D$ is the in-plane gap length between grains. Generally λ will be a tensor that depends on the direction of current, but for simplicity we will treat it here as a simple scalar. An exponential decay of spin polarized electron flux is consistent with the diffusion of polarized electrons within the nonmagnetic separation layers. Such a variation has been observed by Dieny *et al.*, in spin-valves [14] and, as explained later, our model applies to spin-valves as a special case.

We assume that the electron flux emanating from a grain will divide in proportion to the areas of the bounding faces of the grain. The relative scattering probabilities of the faces depend on the amount of electron flux through them. The area of a side face is equal to tD and that of a bottom or top face of a grain is D^2, thus the electron flux will divide between the side, and bottom or top faces as $tD/(tD + D^2)$ and $D^2/(tD + D^2)$ respectively. The scattering probabilities are thus further modified by these factors.

The fraction of the terminal electron flux that actually impinges on a neighboring surface is determined by an

incidence cross section in the direction of electron flow. We define incidence cross sections for intralayer and interlayer scattering as shown in Fig. 3(b,c). Each incidence cross section spans the area occupied by a grain and its nonmagnetic boundary region up to the nearest neighbors of the grain. The fraction of the area of the incidence cross section that is occupied by magnetic material affects the scattering probability of electrons at the grain surface. The scattering probabilities are therefore multiplied further by these fractions which are equal to $tD/(2A - D)(2d + t)$ and $D^2/(2A - D)^2$ for intralayer and interlayer scattering. Evidently these factors are proportional to the packing factor $p = (D/A)^2$ of a magnetic layer (the fraction of the surface area of a film that is occupied by magnetic material). With these considerations in mind, the scattering parameters for a grain of an internal magnetic layer can now be expressed as

$$\alpha_r = \left\{\frac{tD}{tD + D^2}\right\}\left\{\frac{tD}{(2A - D)(2d + t)}\right\} e^{-g/\lambda} = Q_r e^{-g/\lambda}, \tag{2}$$

and

$$\alpha_I = \left\{\frac{D^2}{tD + D^2}\right\}\left\{\frac{D^2}{(2A - D)^2}\right\} e^{-d/\lambda} = Q_I e^{-d/\lambda}, \tag{3}$$

where $\mathbf{Q}_r$, $\mathbf{Q}_I$ are the geometric parts of the scattering parameters. The intralayer scattering cross section for the first and last magnetic layers of a multilayer film, is roughly half of that shown in Fig. 3(b). For these layers a geometric factor $tD/[(2A - D)(d + t)]$ should be used instead in (2).

The formulation given above attributes identical scattering mechanisms to intralayer and interlayer scattering. The effectiveness of these components depends on the microstructural geometric properties of the medium. For media with oblate grain shapes, having $D >> t$, the interlayer scattering component dominates the intralayer component. Such is the case for annealed NiFe/Ag multilayer films. Thus, using the typical values for annealed NiFe/Ag multilayer films of $D = 50$ nm, $A = 51$ nm, $t = 2$ nm, and $d = 4$ nm in (2) and (3) yields $Q_r/Q_I = 0.008$. These values are typical of those used in the simulations presented in this article. Consequently, the intralayer term in (1) can be neglected to obtain

$$\rho = \rho_s + \delta\rho_I = \rho_s[1 + \chi_I \alpha_I (1 - \hat{\mathbf{m}}_0 \cdot \hat{\mathbf{m}}_5)]. \tag{4}$$

Given a magnetization distribution of the medium, the grain resistances obtained with (1) or (4) are used in an equivalent electrical circuit as shown in Fig. 4 to obtain the total resistance of the medium. The magnetization distribution in the medium depends on the external applied field, the relative strengths of the internal magnetic interactions (magnetostatic, exchange, anisotropic etc.) and the history of the magnetization process [12]. As the number of magnetic layers increases, the effects of long-range magnetostatic interactions become increasingly important. The layering of the electrical equivalent circuits will also change to reflect the additional magnetic layers. A glossary of the variables appearing in the formulation of the micromagnetic model is given in the appendix.

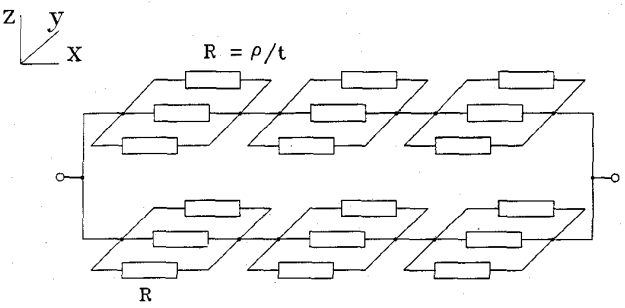

Fig. 4. Equivalent electrical circuit for the current-in-plane direction, used in the micromagnetic model to represent the effects of scattering between an adjacent pair of magnetic layers. The figure illustrates a hypothetical medium in which each magnetic layer is composed of a 3 × 3 array of grains.

III. Large-Scale Model

We now formulate a large-scale phenomenological model that approximates the micromagnetic model in the case when the dominant scattering is interlayer scattering. As before, we consider films having magnetic layers of equal thicknesses and identical interlayer separations. Minor modifications to the theory can be made to extend it to films with unequal magnetic layers and different separations. We begin with an expression for the mean resistivity ρ_m of a magnetic layer. This expression is formally chosen to resemble (4):

$$\rho_m(H) = \langle\rho_s\rangle + \delta\rho_m = \langle\rho_s\rangle\{1 + \chi\alpha[1 - C(H)]\}, \tag{5}$$

where

$$\alpha = \frac{\langle D^2\rangle}{\langle(2A - D)^2\rangle} e^{-d/\Lambda}. \tag{6}$$

In (5) and (6), $\langle\rho_s\rangle$ is the mean resistivity at saturation of a magnetic layer, α is an interlayer scattering parameter, $\delta\rho_m$ is mean resistivity change, C is a mean interlayer magnetization correlation coefficient that expresses the degree of alignment between the magnetization of adjacent magnetic layers, Λ is a characteristic electron scattering length, χ is a material-dependent cofactor, and the notation $\langle..\rangle$ denotes averaging. Scattering length Λ is assumed to be independent of annealing conditions for all the samples obtained from the same unannealed continuous multilayer film base. In the context of the micromagnetic model, parameter C represents a correlation factor c defined as $c = (\Sigma_{N-1}\langle\hat{\mathbf{m}}_0 \cdot \hat{\mathbf{m}}_5\rangle)/(N - 1)$, where the outer summation in the numerator is over the $N - 1$ interlayer regions of a film of N magnetic layers. C and c vary between the values $+1$ and -1 corresponding to the complete parallel and antiparallel orientation of the magnetization of the layers. An equivalent circuit of the large-scale model in the CIP direction is illustrated in Fig. 5.

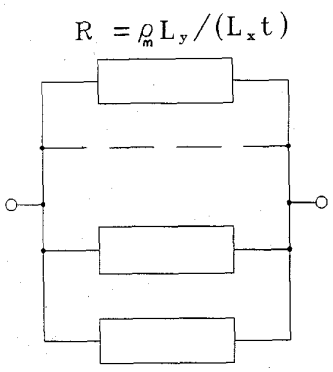

Fig. 5. An equivalent electrical circuit used in the large-scale model for representing the effects of interlayer scattering in the current-in-plane direction.

The resistance of a magnetic layer is given by $\rho_m L_y/(L_x t)$, where L_x and L_y are the lengths of the active area of the sample along the x and y axes.

The linear dimensions appearing in (6) can be obtained from experimental microstructural analyses of the sample such as its transmission electron micrograph. The dimensions of the sample whose GMR response is the dominant GMR curve, are used to obtain Λ. The additional subscript d is used below to denote the parameters of the dominant GMR curve. An approximate value for the scattering parameter α_d of the dominant GMR curve is found by assuming that the maximum correlation factor of the dominant GMR curve $C_{\max,d}$, is equal to the antiparallel value of -1. We write for the dominant curve

$$\left(\frac{\Delta R}{R}\right)_{\max,d} = \frac{R_{\max,d}}{R_{s,d}} - 1 = \chi\alpha_d(1 - C_{\max,d}), \quad (7)$$

from which follows

$$\alpha_d = \frac{1}{\chi(1 - C_{\max,d})}\left(\frac{\Delta R}{R}\right)_{\max,d} \approx \frac{1}{2\chi}\left(\frac{\Delta R}{R}\right)_{\max,d}. \quad (8)$$

Making the substitution $\alpha = \alpha_d$ in (6) and solving for Λ we obtain

$$\Lambda = \frac{d}{\ln\left(\frac{1}{\alpha_d}\frac{\langle D^2\rangle}{\langle(2A - D)^2\rangle}\right)}. \quad (9)$$

Λ obtained from the dominant curve data can now be used in (6) to obtain estimates of α for the other samples. These values of α will be different from each other because of the differences in the microstructural geometric properties of the samples. The variation of the correlation factor of a sample with applied magnetic field is obtained from (5), from knowledge of α and the GMR response curve, $\Delta R/R(H)$:

$$C(H) = 1 - \frac{\Delta R}{R}(H)\frac{1}{\alpha}. \quad (10)$$

Other functional dependencies besides an exponent can be used to model the spatial attenuation of electron flux, and other variations to the models are possible with regard to considered equivalent electrical circuits and the definitions of scattering cross sections. The theory is also applicable to spin-valve structures. In this case, the lengths A and D are equal, and any GMR response curve can serve as the dominant curve. For exponential flux attenuation and fixed lengths t and d of the magnetic layers, the expression for the scattering parameter of the large-scale model reduces to

$$\alpha = e^{-d/\Lambda} \quad (11)$$

For spin valves, the form of the spatial attenuation of the electron flux is given experimentally by the dependence of the GMR amplitude on interlayer separation d. If the value C for a particular field is known, this can be used with the measured mean resistivity ρ_m (at the given field) in (5) to obtain χ. A glossary of the variables appearing in the formulation of the large-scale model is given in the Appendix.

IV. Simulation and Experiment

The micromagnetic model was applied to double-layer (NiFe/Ag/NiFe) films whose magnetization distributions were obtained using a previously described double-layer magnetization model [12]. In the magnetization model, each magnetic layer is simulated by a rectangular array of discrete parallelopiped elements representing the grains of the layers as shown in Fig. 2. Each grain has a fixed magnitude magnetic moment which is allowed to dynamically relax (in three dimensions) in the presence of an external field, an effective exchange field, an effective anisotropy field and a magnetostatic field. The magnetic layers are characterized by distributions of exchange, anisotropy, and magnetostatic parameters among the grains. All the simulation results presented in this article were obtained for a grain size D of 50 nm, a magnetic layer thickness t of 2 nm, and an interlayer separation d of 4 nm. The magnitudes of the magnetization of the grains were selected at random from a 50 kA/m interval centered about a mean value of 500 kA/m. This introduces some inhomogeneity in the magnetic properties of the grains. Each grain had a uniaxial crystalline anisotropy of strength 5×10^2 J/m^3, and the anisotropy easy axes were oriented randomly among the grains. Cofactor values $\chi = \chi_r = \chi_I = 1$, were used for all the simulations presented in this article.

The contribution $\Delta\mathbf{H}_{ex}$ to the effective exchange field acting on a grain of magnetization $\mathbf{M}$ due to a nearest neighbor of magnetization $\mathbf{M}_b$, a distance w from it, is calculated using the expression [12]

$$\Delta H_{ex} = \frac{A^* e^{-\xi w}}{MA^2}\hat{\mathbf{m}}_b, \quad (12)$$

where A^* is a phenomenological exchange parameter. For intralayer exchange interactions $w = A - D$, and for interlayer exchange interactions $w = t$. The parameter ξ is arbitrarily chosen such that the exchange strength de-

creases tenfold over a distance equal to the exchange length $l = (2A^*/M^2)^{1/2}$, that is by setting $A^*e^{-\xi l} = 0.1A^*$. This simulates the expected reduction in exchange coupling between the grains as the gap between them increases.

Each magnetic layer was simulated by a 20 × 20 array of elements yielding active sample areas of roughly 1 × 1 μm. Continuity of the sample along the y axis was modeled by imposing periodic boundary conditions in this direction. An initial magnetization distribution was created in the sample by allowing it to relax starting from a uniformly magnetized state in the y direction with no external field applied. A gradually increasing uniform transverse field (parallel to the x axis) was then applied to the sample up to 40 kA/m. The field was then gradually reduced to 0 and increased in the negative direction up to 40 kA/m. GMR response curves plotted in this article are for field excursions from 40 kA/m to −40 kA/m.

The large-scale model was tested by applying its equations to GMR response curves obtained using the micromagnetic model and seeing how well it predicted media characteristics deliberately fed into the micromagnetic model. Exchange interactions were neglected in these calculations. Media dimensions corresponding to the physically relevant condition $d/\lambda < 1$ (which is necessary for the observation of GMR) were considered. In this calculation, the GMR curves obtained with the micromagnetic model for each specified λ, were treated as dominant GMR curves. The corresponding α_d values for each curve obtained using (8) were then used in (9) to obtain Λ. The micromagnetic model was used to calculate the increase in GMR response, as λ increased. Values of Λ calculated using (9) for gap lengths $g = 1.5$ nm and 5 nm are listed in Table I together with the values of λ used as inputs in the micromagnetic model. The maximum correlation factor $c_{\max}$ using the micromagnetic model, that is obtained for the $g = 1.5$ nm sample is 0.81, and is −1.0 for the $g = 5$ nm sample. The latter value was assumed in deriving (9), and, as seen in Table I, the error incurred is smaller for Λ calculated from this sample.

The maximum correlation factors calculated with the micromagnetic model for different media packing factors (corresponding to varying gap length g), using $\lambda = 5$ nm, are compared with those predicted by the large-scale model in Table II. These calculations were carried out by using as the dominant curve, the GMR response curve of the $g = 1.5$ nm media. This is the dominant curve of a set of curves obtained in simulating the effects of annealing, as discussed in the next section. The remanent magnetization distribution in this sample is shown in Fig. 6. As seen in the figure, away from the edges of the device, the magnetization of grains in corresponding locations in the magnetic layers tends to align antiparallel to each other. This reduces the total magnetostatic energy of the sample. Edge pinning effects prevent the antiparallel orientation of magnetization of the edge grains. The Λ calculated from the dominant curve ($\Lambda = 4.8$ nm in Table I) was used in (6) to obtain a set of α values that were used

TABLE I
COMPARISON OF SCATTERING LENGTHS: λ IS SPECIFIED IN THE MICROMAGNETIC MODEL AND TWO SETS OF Λ ARE PREDICTED USING THE LARGE-SCALE MODEL FOR MEDIA WITH INTERGRANULAR GAP LENGTHS OF g = 1.5 nm AND 5 nm.

λ, nm	g = 1.5 nm		g = 5.0 nm	
	Λ, nm	Error, %	Λ, nm	Error, %
4	3.7	7.5	4.0	0
5	4.8	4.0	4.9	2.0
7	6.5	7.1	6.8	2.8
10	9.0	10.0	9.7	3.0
12	10.6	11.6	11.6	3.3
15	12.9	14.0	14.4	4.0

TABLE II
COMPARISON OF MAXIMUM CORRELATION FACTORS CALCULATED USING THE MICROMAGNETIC MODEL $c_{\max}$ AND THE LARGE-SCALE MODEL $C_{\max}$ FOR DIFFERENT INTERGRANULAR GAP LENGTHS g.

g, nm	c_{max}	C_{max}
0.5	0.63	0.55
1.0	-0.55	-0.72
1.5	-0.81	-1
5.0	-1	-1.1
10.0	-1	-1.2

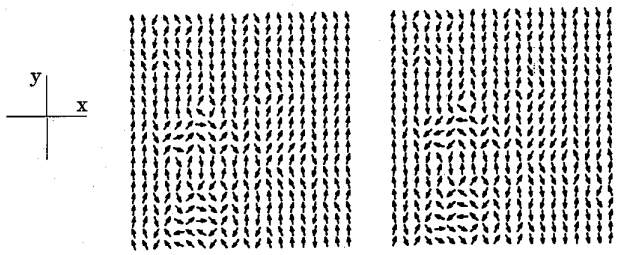

Fig. 6. Remanent magnetization distributions in the magnetic layers of a double-layer medium having an intergranular gap length of $g = 1.5$ nm. The arrows represent the projections of the magnetization vectors of the grains in the x-y plane.

in (10) to obtain $C_{\max}$ for the different samples. The predicted maximum correlation factors $C_{\max}$ are less than their exact values in view of the underestimation of C inherent in the derivation of (10); unrealistic correlation factors are even predicted for $g = 5$ nm and 10 nm. In practice, such unrealistic results offer a means of modifying $C_{\max,d}$ in (8) to obtain better predictions. To achieve this, $C_{\max,d}$ should be replaced by $1/C_o$ in (8), where C_o is the maximum unrealistic C value obtained in the initial calculation (such as $C_o = -1.2$ in Table II). Correlation factor profiles calculated with the micromagnetic magnetization model and predicted with the large-scale model are plotted in Fig. 7 for a sample having $g = 1$ nm.

V. MODELING EFFECTS OF ANNEALING

The micromagnetic model was used to simulate the probable effects of annealing on the microstructure of a

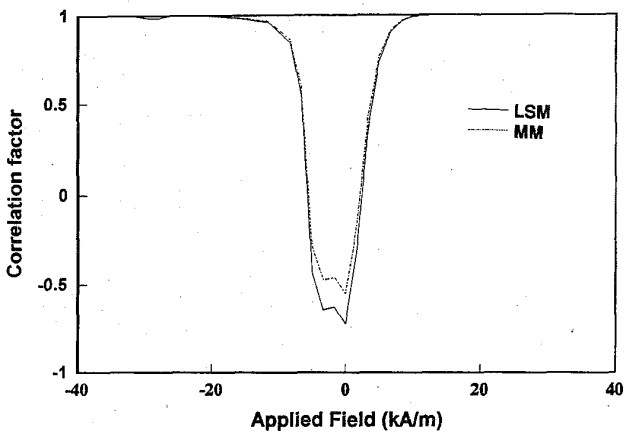

Fig. 7. Correlation factor profiles calculated with the large-scale model (LSM) and micromagnetic model (MM) for double-layer medium having an intergranular gap length of $g = 1.0$ nm.

double-layer film. To first order, the effect of increased annealing can be simulated by assuming that the grain size remains unchanged while the gap length g increases with anneal temperature. Figure 8(a) shows GMR response curves of a double-layer film calculated with the micromagnetic model, using (4), for gap lengths $g = 0.5$, 1.5 and 5 nm and no exchange interaction between the grains. A characteristic length $\lambda = 5$ nm was used in the calculations. Figure 8(b) shows a plot of the amplitude of the response curves as a function of gap length. In this figure the ball-like plot symbols represent data obtained for samples in which was absent intergranular exchange interaction. As seen from the plots, the amplitude of the response curve first increases with g, attaining a maximum at about $g = 1.5$ nm before decreasing with further increase in g, and the width of the response curve increases with g. The increasing misalignment of the remanent magnetization of the layers with increasing g (Fig. 6), accounts for the initial rise in the curve of Fig. 8(b). Beyond $g = 1.5$ nm the effect of less frequent interlayer scattering due to decreased packing factor of the medium, begins to surpass the effect of magnetization misalignment leading to a fall in the amplitude curve. Reduced cooperative switching of grains (and thus the manifestation of individual grain rotation) as g increases is responsible for the broadening of the response curves with increasing g.

This model of annealing ignores the impact on media microstructure of an expected conservation of media volume, especially at large gap lengths. A more plausible explanation of the effects of annealing is perhaps that the gap length ceases to grow beyond a certain value, while the bridging of magnetic grains of neighboring layers across the nonmagnetic spacer layers sets in, intensifying with increased annealing [15]. This may result in increases in the effective ferromagnetic exchange interactions between the magnetic layers. We simulate this effect by obtaining the initial rise of the plot of Fig. 8(b) as before, and then by keeping g fixed at 1.5 nm, gradually increasing ferromagnetic exchange coupling between the

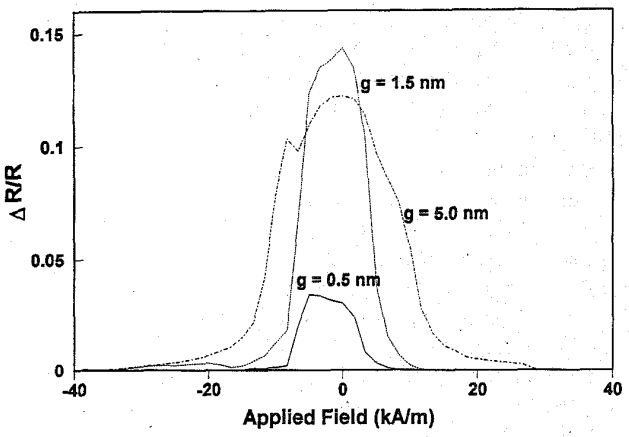

(a)

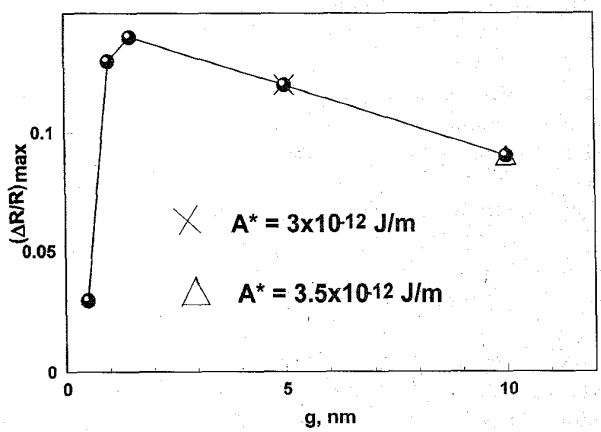

(b)

Fig. 8. (a) GMR response curves obtained with the micromagnetic model for gap lengths $g = 0.5$, 1.5 and 5 nm; (b) amplitude of GMR response curves as a function of gap length obtained with the micromagnetic model, for films having no exchange interactions (represented by ball-like plot symbols). Also plotted are points obtained for films with gap length $g = 1.5$ nm and interlayer exchange coupling strengths A^* of 3×10^{-12} J/m and 3.5×10^{-12} J/m.

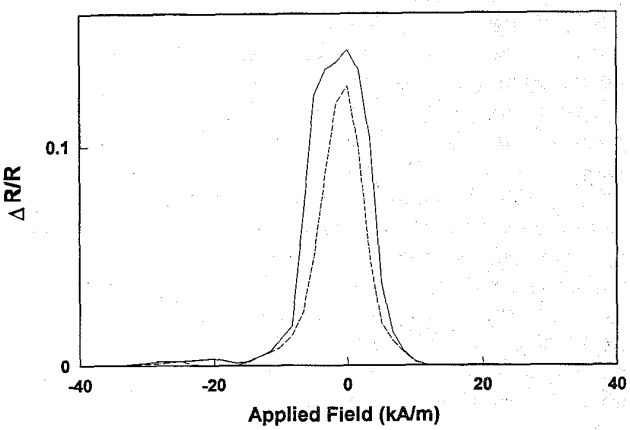

Fig. 9. GMR response curves obtained with the micromagnetic model for a gap length of $g = 1.5$ nm in the absence of exchange interactions (solid curve) and for an interlayer exchange coupling strength of $A^* = 3 \times 10^{-12}$ J/m.

magnetic layers. The values of interlayer exchange constants A^* shown in Fig. 8b are those that yield GMR amplitudes that coincide with the plotted ones obtained with the first model of the effects of annealing. The widths of the response curves decreases with increasing A^* accompanied by a corresponding increase in sensitivity (Fig. 9). Thus, to simulate the broadening of response curves, grain anisotropy strength or g should be increased somewhat. A^* is expected to increase with decreasing interlayer separation d. A behavior similar to that described above was recently reported in NiFe/Ag multilayer films in which d was systematically varied [2]. The existence of grain clusters and nonmagnetic voids in the magnetic layers may affect the GMR responses in other ways.

VI. Summary

We have described magnetization-dependent micromagnetic and large-scale models of GMR in granular-multilayer magnetic films. Our formulation incorporates the interplay between the microstructural and transport properties of the films. The micromagnetic model offers a detailed picture of how the magnetization inside the films affects GMR response. The large-scale model, which is applicable to samples with oblate grains, is useful for obtaining important media parameters from experimental data. The parameters of the models are determined from independent measurements of GMR response curves and the microstructural dimensions of the films. When applied to the response curves generated by the micromagnetic model, the large-scale model accurately predicts media parameters deliberately fed into the micromagnetic model. Both models were used to study experimental temperature-annealed NiFe/Ag films. The micromagnetic model consistently replicated known trends in the GMR behavior of the films for different annealing conditions and film dimensions.

Appendix

This appendix contains a glossary of variables that are used in the formulation of the models described in the text. Two sets of variables are given for the micromagnetic and large-scale models. The variables for the large-scale model are divided into input variables to be determined by experiments, and output variables to be obtained by the model.

Micromagnetic Model

D	grain size
A	distance between centers of adjacent grains within magnetic layer
t	thickness of magnetic layer
d	separation between adjacent magnetic layers
ρ	resistivity of grain
ρ_s	resistivity of grain at saturation
χ_r	material-dependent intralayer cofactor (see (1))
χ_I	material-dependent interlayer cofactor (see (1))
$\delta\rho_r$	intralayer resistivity change
$\delta\rho_I$	interlayer resistivity change
α_r	intralayer scattering parameter
α_I	interlayer scattering parameter
λ	model-dependent electron characteristic transport length
g	gap length between grains within a magnetic layer
Q_r	geometric factor of α_r
Q_I	geometric factor of α_I
A^*	exchange constant
$\mathbf{M}$	magnetization vector
$\hat{\mathbf{m}}$	unit magnetization vector
l	exchange length
c	correlation factor of magnetization between the magnetic layers
ξ	exchange exponential parameter
$\Delta R/R$	relative change in resistance (GMR response)

Large-scale Model

Inputs

$\langle D\rangle$	Average grain size
$\langle A\rangle$	Average distance between centers of adjacent grains within magnetic layer
d	same meaning as indicated above
ρ_m	mean resistivity of magnetic layer
$\langle\rho_s\rangle$	mean resistivity of magnetic layer at saturation
$\delta\rho_m$	change in mean resistivity of magnetic layer
χ	material-dependent co-factor (see (5))
α	interlayer scattering parameter
t	same meaning as indicated above
L_x, L_y	lengths along the x and y axes of active region of sample

Outputs

C	correlation factor of magnetization between magnetic layers
Λ	model-dependent electron characteristic transport length
$\Delta R/R$	same meaning as indicated above

References

[1] T. L. Hylton, K. R. Coffey, M. A. Parker, and J. K. Howard, "Giant magnetoresistance at low fields in discontinuous NiFe-Ag multilayer thin films," *Science*, vol. 261, p. 1021, 1993.

[2] J. Mouchot, P. Gerard, and B. Rodmacq, "Magnetoresistive sensors based on $Ni_{81}Fe_{19}$/Ag multilayers," *IEEE Trans. Magn.*, MAG-29, pp. 2732–2734, 1993.

[3] S. Hossain, D. Seale, G. Qiu, J. Jarratt, J. A. Barnard, H. Fujiwara, and M. R. Parker, "Hysteresis reduction in NiFeCo/Cu multilayers exhibiting large low-field giant magnetoresistance," *J. Appl. Phys.* vol. 75, pp. 7067–7069, 1994.

[4] R. L. White, "Giant magnetoresistance: A primer," *IEEE Trans. Magn.* MAG-28, pp. 2482–2487, 1992.

[5] S. S. P. Parkin, N. More and K. P. Roche, "Oscillations in exchange coupling and magnetoresistance in metallic superlattice structures: Co/Ru, Co/Cr, and Fe/Cr," *Phys. Rev. Lett.*, vol. 64, pp. 2304–2307, 1990.

[6] J. C. Slonczewski, "Magnetostatic mechanism for field-sensitivity of magnetoresistance in discontinuous magnetic multilayers," *J. Magn. Magn. Mat.*, vol. 129, pp. L123–L128, 1994.

[7] M. N. Baibich, J. M. Broto, A. Fert, F. Nguyen Van Dau, F. Petroff, P. Etienne, G. Cruezet, A. Frederick, and J. Chazelas, *Phys. Rev. Lett.* vol. 61, p. 2472, 1988.
[8] S. Zhang, P. M. Levy and A. Fert, "Conductivity and magnetoresistance of magnetic multilayered structures," *Phys. Rev. B*, vol. 45, pp. 8689–8702, 1992.
[9] B. Dieny, V. S. Speriosu, S. S. P. Parkin, B. A. Gurney, D. R. Wilhoit, and D. Mauri, "Giant magnetoresistance in soft ferromagnetic multilayers," *Phys. Rev. B*, vol. 43, p. 1297, 1991.
[10] S. F. Lee, W. P. Pratt, Jr., R. Loloee, P. A. Schroeder, and J. Bass, "Field-dependent interface resistance" of Ag/Co multilayers," *Phys. Rev. B*, vol. 46, pp. 548–551, 1992.
[11] S. W. Yuan and H. N. Bertram, "Micromagnetics of GMR spin-valve heads," *J. Appl. Phys.* vol. 75, 6385–6387, 1994.
[12] J. O. Oti, "A micromagnetic model of dual-layer magnetic recording thin-films," *IEEE Trans. Magn.* MAG-29, p. 1265, 1993.
[13] R. W. Cross, S. E. Russek, S. C. Sanders, M. R. Parker, J. A. Barnard, and S. A. Hossian, "Size and self-field effects in giant magnetoresistive thin film devices," *IEEE Trans. Magn.*, in press.
[14] B. Dieny, V. S. Speriosu, S. Metin, S. S. P. Parkin, B. A. Gurney, P. Baumgart and D. R. Wilhoit, "Magnetotransport properties of magnetically soft spin-valve structures," *J. Appl. Phys.* vol. 69, p. 4774, 1991.
[15] T. L. Hylton, K. R. Coffey, M. A. Parker and J. K. Howard, "Low field giant magnetoresistance in discontinuous magnetic multilayers," *J. Appl. Phys.* vol. 75, p. 7058, 1994.

John Oti received the M.Sc. (E.E.) degree from Vorshilovgrad Machine-Building Institute, Ukraine, in 1984, and the D.Sc. degree in Engineering from George Washington University in 1991.

From 1991 till 1993 he was a NIST/ASEE Postdoctoral Research Fellow at the National Institute of Standards and Technology, Boulder, Colorado. During the summers of 1988, 1989 and 1990 he was a member of the research staff in The Thin Film Department at Hewlett-Packard Laboratories, Palo Alto California, where he designed read-write models of magnetic recording. His current research interests include the micromagnetic characterization of multilayer magnetic recording thin films and giant magnetoresistance multilayers, and magnetic interactions in magnetic force microscopy.

Stephen E. Russek received the A.B. degree in physics from Harvard University in 1980 and a Ph.D. degree in physics from Cornell University in 1990. He spent the two years between undergraduate and graduate school working at AT&T Bell Laboratories doing research in silicon device physics. His graduate studies at Cornell included work on Nb based tunnel junctions at low temperatures (10 mK – 100 mK), development of in-situ growth of high Tc superconductors, and a study of superconducting grain boundary weak-link devices.

After a two year NRC post doctoral fellowship at NIST, Boulder he joined the permanent staff at NIST in the Superconductor and Magnetic Measurements group in January 1992. He is presently the leader of the Magnetic Recording Metrology Project and specializes in magnetic thin film device fabrication and measurements. His current research projects include the development of a magnetic imaging standard, studying the size effects in submicrometer GMR sensors for use in MRAM, recording heads, and imaging sensors, and the development of novel measurement systems for the magnetic data storage industry.

Steven C. Sanders received the B.A. degree from Augustana College (IL) and the Ph.D. degree in Physics from Iowa State University in 1992. He completed a two year NRC postdoctoral fellowship at the National Institute of Standards and Technology prior to joining the scientific staff. His current research focuses on the processing and properties of magnetic multilayer thin films. Other research interests include electronic transport at superconducting-metal interfaces. He is a member of the American Physical Society and the Materials Research Society.